COMMUNICATION

Vacancy Effect on Electrocatalytic Activity of $LaMn_{½}Co_{½}O_{3-δ}$ for Hydrogen and Oxygen Evolution Reactions

Received 00th January 20xx,
Accepted 00th January 20xx

DOI: 10.1039/x0xx00000x

Md. Sofiul Alom[a], Farshid Ramezanipour[a,*]

Development of enhanced electrocatalysts for water splitting can be a significant step toward green hydrogen generation. In this work, a remarkable enhancement of electrocatalytic properties is achieved through incorporation of oxygen-vacancies in a perovskite oxide, while maintaining the same structural framework. The oxygen-deficient material $La_2MnCoO_{6-δ}$ ($LaMn_{0.5}Co_{0.5}O_{3-δ}$) is isostructural to the parent stoichiometric material, but shows drastically enhanced electrocatalytic properties for both half-reactions of water-splitting, namely hydrogen-evolution and oxygen-evolution reactions, due to the oxygen-vacancies.

A promising method of hydrogen production is the electrochemical water splitting, which involves two half reactions, oxygen evolution reaction (OER) and hydrogen evolution reaction (HER). Sluggish kinetics of these reactions, especially OER, presents a major challenge and results in considerable overpotential. To address this problem, precious metal catalysts, such as Pt/C for HER, and IrO_2 and RuO_2 for OER have been traditionally used. However, due to their high cost and low abundance, there is need for more economical and earth abundant alternatives. Perovskite oxides,[1,2] a class of transition metal oxides, have shown great promise for electrochemical water splitting.[3-8] The general formula of this class of materials is ABO_3 (or $A_2B_2O_6$ when more than one A or B metal is present). The A-site often contains alkaline-earth or lanthanide cations, and the B-site is usually occupied by transition metal cations. The A site cations reside in spaces between BO_6 octahedral units. The electrocatalytic activities of these materials can be modified by varying the A and B-site metals.[3-8] For example, in the perovskite series $CaSrFe_{1-x}Co_{1-x}Mn_{2x}O_{6-δ}$, the transition metal ratios, located at the B-site, have been varied to find the best OER activity in x = 0.25 phase.[3] Changes in the A-site can also affect the electrocatalytic properties, as demonstrated for the series $Ca_{2-x}Sr_xFeMnO_{6-δ}$ (x = 0, 1, 2), where the x = 1 phase shows the best HER and OER activities in the series.[6]

Another approach for the modification of the electrocatalytic properties is the incorporation of oxygen-vacancies, which can also be achieved by metal substitution, as reported for $La_{1-x}Sr_xFeO_{3-δ}$.[2] In this compound, gradual substitution of La^{3+} by Sr^{2+} results in an increase in the concentration of oxygen vacancies, where the x = 0.8 phase shows the best OER activity. However, this type of metal substitution also has an additional effect, that is an increase in the average oxidation state of iron, which together with oxygen vacancies, help to resolve the charge imbalance arising from the substitution of the trivalent La^{3+} by divalent Sr^{2+}.[2] As a result, more than one parameter contribute to the change in electrocatalytic properties. Therefore, the improvement of the OER activity cannot be attributed only to oxygen-vacancies. However, it is possible to create oxygen-vacancies in transition metal oxides, without the need for metal substitution, where the vacancies are created by controlled reduction. For example, various methods of the formation of oxygen-vacancies in titanium oxide-based nanostructures have been recently studied.[9]

In the present work, we apply this approach to the development of electrocatalysts for water-splitting. We demonstrate a remarkable enhancement of electrocatalytic properties upon incorporation of oxygen-vacancies in La_2MnCoO_6 ($LaMn_{0.5}Co_{0.5}O_3$), to form an isostructural oxygen-deficient perovskite, $La_2MnCoO_{6-δ}$ ($LaMn_{0.5}Co_{0.5}O_{3-δ}$), which shows superior activity for both HER and OER. The parent material was synthesized through sol-gel method, and was then reduced using 10% H_2 in argon. Iodometric titrations confirmed full oxygen

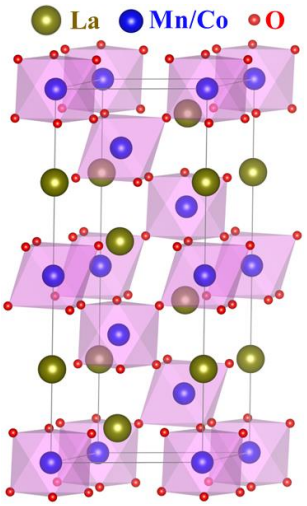

Figure 1. Crystal structure of $LaMn_{0.5}Co_{0.5}O_3$.

[a] Department of Chemistry, University of Louisville, Louisville, KY 40292, USA.
*Email: farshid.ramezanipour@louisville.edu, Phone: +1(502) 852-7061
ORCID: 0000-0003-4176-1386

Electronic Supplementary Information (ESI) available: Experimental procedures and supplementary figures. See DOI: 10.1039/x0xx00000x

Please do not adjust margins

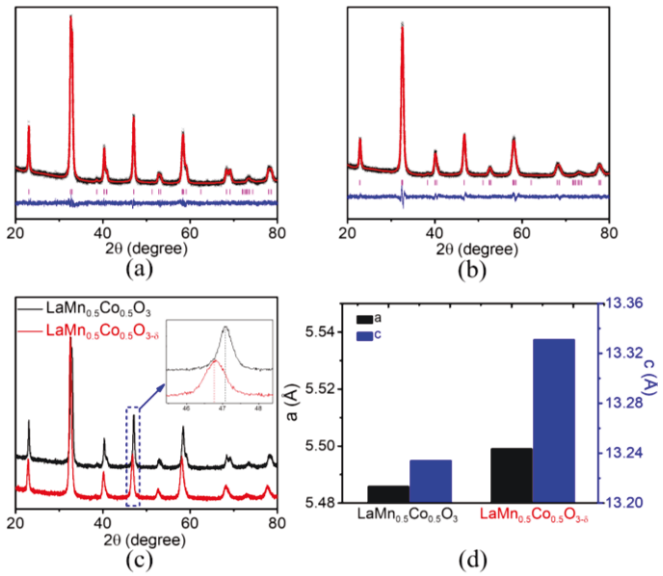

Figure 2. Rietveld refinement profiles for powder X-ray diffraction (PXRD) data of (a) $LaMn_{0.5}Co_{0.5}O_3$ and (b) $LaMn_{0.5}Co_{0.5}O_{3-\delta}$. (c) Comparison of PXRD data, indicating the peak shift. (d) Comparison of the unit cell dimensions *a* (black) and *c* (blue).

stoichiometry of $LaMn_{0.5}Co_{0.5}O_3$ and the creation of oxygen-vacancies in $LaMn_{0.5}Co_{0.5}O_{3-\delta}$ (δ = 0.1). Detailed experimental procedures are provided in the supporting information. Rietveld refinements using X-ray diffraction data confirm that the parent material has a trigonal R $\bar{3}$c structure, comprising corner-sharing $(Mn/Co)O_6$ octahedra (Figure 1 and Table S1), consistent with previous reports of its structure.[10, 11] The oxygen-deficient analogue also has the same structure, as confirmed by Rietveld refinements (Figures 2). The two materials also have similar microstructures and grain sizes, as evident from scanning electron microscopy (SEM) images in Figure S1. However, the unit cell of the oxygen-deficient material is larger than that of the parent non-deficient phase (Figures 2d), as observed from the shift of diffraction peaks toward lower 2θ, consistent with the inverse relation of *d*-spacing with diffraction angle from Bragg's law $d = n\lambda/2\,sin\theta$. The unit cell dimensions and refined structural parameters are shown in Figure 2d and Table S2. The larger unit cell indicates the partial reduction of trivalent transition metals into larger divalent ions, to allow the formation of oxygen-vacancies. The XPS spectra of Mn 2p and Co 2p for both materials are shown in Figures 3. The Mn spectrum for $LaMn_{0.5}Co_{0.5}O_3$ is consistent with Mn^{3+}, with $2p_{3/2}$ peak at 641.8 eV and $2p_{1/2}$ peak at 653.3 eV.[12-14] However, for $LaMn_{0.5}Co_{0.5}O_{3-\delta}$ the Mn $2p_{3/2}$ and $2p_{1/2}$ peaks are shifted slightly toward lower binding energies, and are best described by the presence of both Mn^{2+} and Mn^{3+}.[12, 14] The Co spectrum for $LaMn_{0.5}Co_{0.5}O_3$ (Figure 3b) is indicative of trivalent cobalt,[15-17] consisting of $2p_{3/2}$ and $2p_{1/2}$ peaks at 779.9 eV and 795.4 eV, respectively, as well as a satellite peak at ~10 mV higher than the $2p_{3/2}$ peak. This satellite peak is a signature of Co^{3+}.[16, 17] However, for $LaMn_{0.5}Co_{0.5}O_{3-\delta}$, the $2p_{3/2}$ and $2p_{1/2}$ peaks shift slightly to lower binding energies, and there are two satellite peaks at ~5 eV and ~10 eV higher than the $2p_{3/2}$ peak,[16, 18] indicating a mixture of Co^{2+} and Co^{3+}.[15, 17] The XPS findings are consistent with iodometric titration and X-ray diffraction results, all confirming the reduction of transition metals and formation of oxygen vacancies.

The presence of oxygen vacancies has a significant influence on electrocatalytic properties. As shown in Figure 4a, the oxygen-deficient material $LaMn_{0.5}Co_{0.5}O_{3-\delta}$ shows enhanced HER performance in 1 M KOH over the stoichiometric compound, $LaMn_{0.5}Co_{0.5}O_3$. The HER onset potential for $LaMn_{0.5}Co_{0.5}O_3$ and $LaMn_{0.5}Co_{0.5}O_{3-\delta}$, taken at 2 $mAcm^{-2}$, are 387 mV and 322 mV, respectively. Here the onset potential was chosen at a specific current density to avoid the variation in onset potential values by different observers.[19, 20] The overpotential required to deliver a current density 10 $mAcm^{-2}$, η_{10}, is a common metric for the comparison of electrocatalytic activities of different catalysts. The η_{10} value for the oxygen-deficient material, $LaMn_{0.5}Co_{0.5}O_{3-\delta}$ (η_{10} = 413 mV) is abount 66 mV lower than that of the parent material, $LaMn_{0.5}Co_{0.5}O_3$ (η_{10} = 479 mV). The HER overpotentials of these catalysts are not as low as those observed for the state-of-the-art catalyst Pt/C (less than 100 mV)[21] or some oxides such as $SrCa_2GaMn_2O_8$ (η_{10} = 315 mV).[22] However, they are lower than those of some other oxides, such as $Sr_2LaCoMnO_7$ (η_{10} = 612 mV)[23] and $Ca_2LaMn_2O_7$ (η_{10} = 595 mV).[24] Nevertheless, the important observation here is the significant decrease in overpotential due to a small degree of oxygen-vacancies. In addition, as shown in the inset of Figure 4a, $LaMn_{0.5}Co_{0.5}O_{3-\delta}$ shows nearly constant chronopotentiometry response for at least 20 hours, indicating its stability during HER.

The relative kinetics of HER was studied using Tafel equation, $\eta = a + b \log j$, where η is the overpotential and j is the corresponding current density.[20] Tafel slope, b, is the slope of the plot of η vs log j (Figure 4b), indicating the reaction kinetics, and impacted by the electron and mass transfer.[25] Faster reaction kinetics is represented by a smaller Tafel slope, signifying the generation of a large current by a small increase in the potential beyond the onset potential.[26] As shown in Figure 4b, the Tafel slopes for $LaMn_{0.5}Co_{0.5}O_3$ and $LaMn_{0.5}Co_{0.5}O_{3-\delta}$ are 167 $mVdec^{-1}$ and 114 $mVdec^{-1}$, respectively. The lower Tafel slope of the latter compound indicates faster reaction kinetics, and is consistent with its higher electrocatalytic performance. The charge transfer resistance in the HER region is also found to be smaller for $LaMn_{0.5}Co_{0.5}O_{3-\delta}$, indicating better charge transfer, as shown in Figure S2a.

The mass activity (MA) was also calculated to assess the intrinsic properties of the catalysts. The equation[27] MA = (j×A)/m, was used to calculate the mass activity in A/g, where j is the current density in $mAcm^{-2}$, A is the geometrical surface area of the GC electrode in cm^2 and m is the amount of catalyst loaded on the GC electrode in mg. The mass activities of $LaMn_{0.5}Co_{0.5}O_3$ and $LaMn_{0.5}Co_{0.5}O_{3-\delta}$ are compared in Figure 4c at different

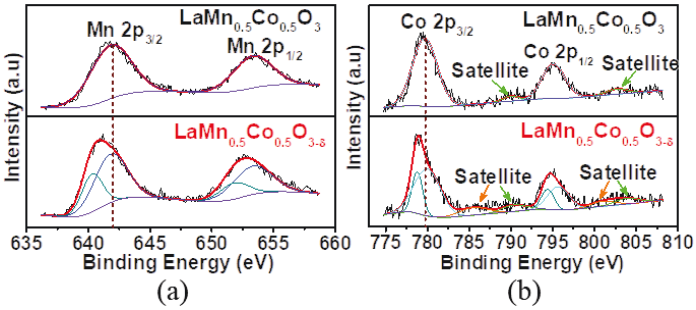

Figure 3. XPS spectra of (a) Mn 2p and (b) Co 2p, showing $LaMn_{0.5}Co_{0.5}O_3$ data in the top panel and $LaMn_{0.5}Co_{0.5}O_{3-\delta}$ at the bottom.

This journal is © The Royal Society of Chemistry 20xx

Please do not adjust margins

Please do not adjust margins

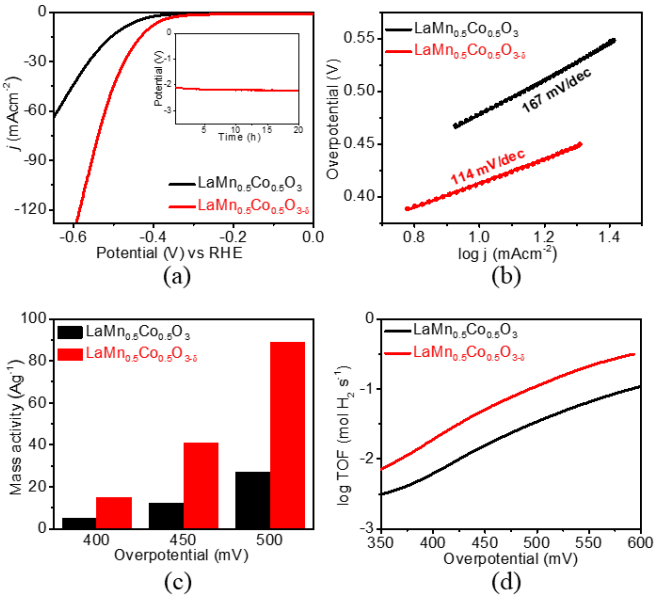

Figure 4. (a) HER polarization curves in 1 M KOH. Chronopotentiometry data for the best catalyst, $LaMn_{0.5}Co_{0.5}O_{3-\delta}$, is shown in the inset. (b) Tafel plots and slopes. (c) HER mass activities at different overpotentials. (d) Plot of log TOF versus overpotential of HER.

overpotentials, showing greater mass activity for the latter material at all overpotentials. The turnover frequency (TOF) was calculated using the equation[28, 29] TOF = ((j×A)/(x×F×n), where j, A, x, F and n are current density ($mAcm^{-2}$), surface area of GC electrode (0.196 cm^2), number of electron transfer to produce one mole of product (2 for HER and 4 for OER), Faraday constant (96485 $A.s.mol^{-1}$) and number of moles of active sites (Mn/Co), respectively. The TOF plots of $LaMn_{0.5}Co_{0.5}O_3$ and $LaMn_{0.5}Co_{0.5}O_{3-\delta}$ are compared in the HER region in Figure 4d. The TOF of the latter is consistently higher than that of the former, consistent with the better HER activity of the oxygen-deficient material.

These materials are also capable of catalyzing the other half-reaction of water-splitting, namely OER. The electrocatalytic activities for OER in 1 M KOH are shown in Figure 5, indicating that the oxygen-deficient material, $LaMn_{0.5}Co_{0.5}O_{3-\delta}$ shows superior OER activity compared to the stoichiometric material, $LaMn_{0.5}Co_{0.5}O_3$. The onset potentials for $LaMn_{0.5}Co_{0.5}O_3$ and $LaMn_{0.5}Co_{0.5}O_{3-\delta}$ at 2 $mAcm^{-2}$ are 1.62 V and 1.54 V, respectively, indicating that OER process can start at a lower potential for the oxygen-deficient material. Importantly, the OER current response at the same potential increases immensely, by more than one order of magnitude. The OER overpotential, η_{10}, is defined as the potential beyond the thermodynamic potential of 1.23 V at 10 $mAcm^{-2}$. The overpotential for $LaMn_{0.5}Co_{0.5}O_3$ is 460 mV, consistent with the values reported for similar compositions.[30, 31] However, the overpotential is drastically decreased, by about 100 mV, when oxygen-deficiencies are incorporated in the material, giving $\eta_{10} \approx 360$ mV for $LaMn_{0.5}Co_{0.5}O_{3-\delta}$. The overpotential of the oxygen-deficient material is lower than that reported for the precious metal catalyst RuO_2 (η_{10} = 400 mV),[32] and those of some other oxide catalysts, such as Co_3O_4 (η_{10} = 400 mV)[33] and $CaSrFeMnO_{6-\delta}$ (η_{10} = 370 mV).[6] In addition, as demonstrated by the chronopotentiometry data in the inset of Figure 5a, $LaMn_{0.5}Co_{0.5}O_{3-\delta}$ shows great stability for at least 20 hours. This material also has enhanced kinetics, indicated by the smaller Tafel slope, obtained from the plot of η vs log j in Figure 5b. The faster reaction kinetics of $LaMn_{0.5}Co_{0.5}O_{3-\delta}$ is consistent with its superior OER activity compared to $LaMn_{0.5}Co_{0.5}O_3$. The former also has a lower charge transfer resistance, shown by the electrochemical impedance spectroscopy data in the OER region (Figure S2b), indicating the enhanced charge transfer.

Mass activities for OER at different overpotentials are shown in Figure 5c, indicating the drastically greater mass activity of $LaMn_{0.5}Co_{0.5}O_{3-\delta}$. The latter shows an almost 9-fold higher OER mass activity compared to $LaMn_{0.5}Co_{0.5}O_3$, at an overpotential of 400 mV. In addition, the OER turnover frequency (TOF) is consistently higher, by nearly one order of magnitude, for the oxygen-deficient material at all overpotentials, as shown in Figure 5d. The structural stabilities of both materials under the electrochemical conditions are shown by the X-ray diffraction data before and after HER and OER (Figure S3). The diffraction patterns remain nearly unchanged after electrocatalytic experiments, indicating that these materials retain their structural integrity, further confirming their stability. The double layer capacitance, C_{dl}, values were also compared for the two materials. The importance of C_{dl} is that it is directly proportional to the electrochemically active surface area.[8] The C_{dl} values were obtained using the equation $C_{dl} = j_{average}/v$, where $j_{average}$ is the average of the absolute values of j_{anodic} and $j_{cathodic}$ from cyclic voltammetry data in the non-faradic region and v is the scan rate. The slope of the plot of $j_{average}$ vs v is equivalent to C_{dl}. Using the non-faradic cyclic voltammetry data in Figures S4a and b, the $j_{average}$ values are obtained at the middle potential of 0.925 V, and are plotted against their corresponding scan rates (Figures S4c). As observed from the slope of this plot, the C_{dl} for the oxygen-deficient material $LaMn_{0.5}Co_{0.5}O_{3-\delta}$ is considerably greater than that of $LaMn_{0.5}Co_{0.5}O_3$.

The findings described above indicate that drastic enhancement of electrocatalytic properties can be achieved through incorporation of oxygen-vacancies into an oxide catalyst. This can be

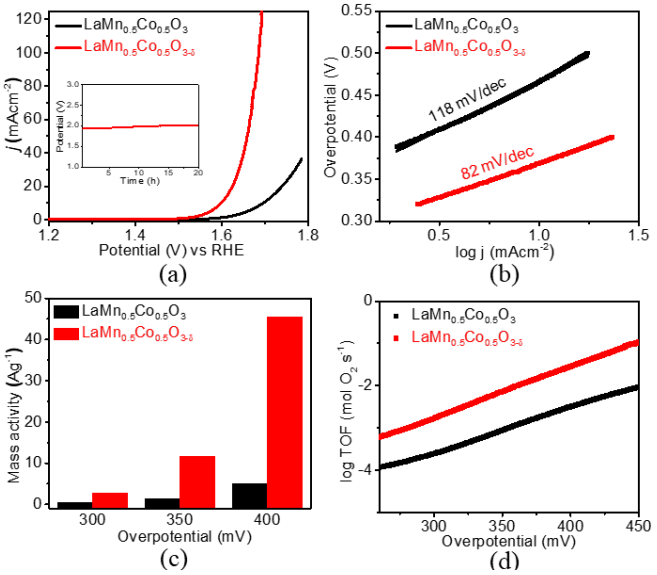

Figure 5. (a) OER polarization curves in 1 M KOH. Chronopotentiometry data for the best catalyst, $LaMn_{0.5}Co_{0.5}O_{3-\delta}$, is shown in the inset. (b) Tafel plots and slopes. (c) OER mass activities at different overpotentials. (d) Plot of log TOF versus overpotential of OER.

Please do not adjust margins

Please do not adjust margins

due to the increase in the adsorption energy of the oxygen-containing intermediates such as H_2O.[34] The oxygen-vacancies result in a decrease in the coordination number of active metal sites, which can make it easier for the incoming reaction intermediates to adsorb on the active sites, leading to an improved electrocatalytic performance.[1, 35-37] The lower charge transfer resistance of $LaMn_{0.5}Co_{0.5}O_{3-\delta}$, observed from the electrochemical impedance spectroscopy in both HER and OER conditions, indicates an improvement in electron transfer due to the presence of oxygen-vacancies. Indeed, this is consistent with theoretical studies that suggest delocalization of the electrons neighboring oxygen-vacancies, which facilitates the electron transport from the reaction interface to the electrodes.[35, 37-40] Thus, oxygen-deficiency can increase both the number of active sites and their reactivity.[34]

Overall, the findings of this study represent an unequivocal example of the impact of oxygen-vacancies, and the ability to enhance the electrocatalytic activity of perovskite oxide catalysts through oxygen-deficiency. The structural framework of the perovskite oxide can be retained while oxygen-vacancies are incorporated into the material, as confirmed by X-ray diffraction, iodometric titrations, and X-ray photoelectron spectroscopy. The presence of oxygen-vacancies results in a remarkable enhancement of electrocatalytic properties for both half-reactions of water-splitting, HER and OER. The drastic decrease in overpotential, by 66 mV for HER and 100 mV for OER, the enhanced reaction kinetics, the significantly superior mass activity and turnover frequency (TOF), by nearly one order of magnitude, highlight the impact of oxygen-vacancies and the effectiveness of this strategy in designing highly active electrocatalysts.

This work is supported by the National Science Foundation (NSF) under grant no. DMR-1943085.

Conflicts of interest

There are no conflicts to declare.

Notes and references

1. J. Kim, X. Yin, K.-C. Tsao, S. Fang and H. Yang, *J. Am. Chem. Soc.*, 2014, **136**, 14646-14649.
2. S. She, J. Yu, W. Tang, Y. Zhu, Y. Chen, J. Sunarso, W. Zhou and Z. Shao, *ACS Appl. Mater. Interfaces*, 2018, **10**, 11715-11721.
3. R. K. Hona, S. B. Karki, T. Cao, R. Mishra, G. E. Sterbinsky and F. Ramezanipour, *ACS Catal.*, 2021, 14605-14614.
4. S. B. Karki, R. K. Hona, M. Yu and F. Ramezanipour, *ACS Catal.*, 2022, **12**, 10333-10337.
5. M. S. Alom, C. C. W. Kananke-Gamage and F. Ramezanipour, *ACS Omega*, 2022, **7**, 7444-7451.
6. R. K. Hona, S. B. Karki and F. Ramezanipour, *ACS Sustainable Chem. Eng.*, 2020, **8**, 11549-11557.
7. S. B. Karki, A. N. Andriotis, M. Menon and F. Ramezanipour, *ACS Appl. Energy Mater.*, 2021, **4**, 12063-12066.
8. R. K. Hona and F. Ramezanipour, *Angew. Chem. Int. Ed.*, 2019, **58**, 2060-2063.
9. A. Sarkar and G. G. Khan, *Nanoscale*, 2019, **11**, 3414-3444.
10. M. Viswanathan, P. S. Anil Kumar, V. S. Bhadram, C. Narayana, A. K. Bera and S. M. Yusuf, *J. Phys.: Condens. Matter*, 2010, **22**, 346006.
11. T. Kyômen, R. Yamazaki and M. Itoh, *Chem. Mater.*, 2003, **15**, 4798-4803.
12. S. B. Karki and F. Ramezanipour, *Mater. Today Chem.*, 2019, **13**, 25-33.
13. P. W. Menezes, A. Indra, V. Gutkin and M. Driess, *Chem. Commun.*, 2017, **53**, 8018-8021.
14. Y. S. Chung, T. Kim, T. H. Shin, H. Yoon, S. Park, N. M. Sammes, W. B. Kim and J. S. Chung, *J. Mater. Chem. A*, 2017, **5**, 6437-6446.
15. Y.-G. Lim, D. Kim, J.-M. Lim, J.-S. Kim, J.-S. Yu, Y.-J. Kim, D. Byun, M. Cho, K. Cho and M.-S. Park, *J. Mater. Chem. A*, 2015, **3**, 12377-12385.
16. J. C. Dupin, D. Gonbeau, H. Benqlilou-Moudden, P. Vinatier and A. Levasseur, *Thin Solid Films*, 2001, **384**, 23-32.
17. D. Gu, C.-J. Jia, C. Weidenthaler, H.-J. Bongard, B. Spliethoff, W. Schmidt and F. Schüth, *J. Am. Chem. Soc.*, 2015, **137**, 11407-11418.
18. N. Davison, W. R. McWhinnie and A. Hooper, *Clays Clay Miner.*, 1991, **39**, 22-27.
19. J. D. Benck, T. R. Hellstern, J. Kibsgaard, P. Chakthranont and T. F. Jaramillo, *ACS Catal.*, 2014, **4**, 3957-3971.
20. M. S. Alom and F. Ramezanipour, *Mater. Chem. Phys.*, 2023, **293**, 126942.
21. C. Wu, D. Liu, H. Li and J. Li, *Small*, 2018, **14**, 1704227.
22. S. B. Karki and F. Ramezanipour, *ACS Appl. Energy Mater.*, 2020, **3**, 10983-10992.
23. C. C. W. Kananke-Gamage and F. Ramezanipour, *Dalton Trans.*, 2021, **50**, 14196-14206.
24. C. C. W. Kananke-Gamage and F. Ramezanipour, *J. Phys. Chem. Solids*, 2022, **171**, 111013.
25. F. Song and X. Hu, *J. Am. Chem. Soc.*, 2014, **136**, 16481-16484.
26. M. S. Alom and F. Ramezanipour, *ChemCatChem*, 2021, **13**, 3510-3516.
27. N. Zhang, X. Feng, D. Rao, X. Deng, L. Cai, B. Qiu, R. Long, Y. Xiong, Y. Lu and Y. Chai, *Nat. Commun.*, 2020, **11**, 4066.
28. X. Lu and C. Zhao, *Nat. Commun.*, 2015, **6**, 6616.
29. V. D. Silva, T. A. Simões, J. P. F. Grilo, E. S. Medeiros and D. A. Macedo, *J. Mater. Sci.*, 2020, **55**, 6648-6659.
30. X. Jiang, Y. Dong, Z. Zhang, J. Li, J. Qian and D. Gao, *J. Alloys Compd.*, 2021, **878**, 160433.
31. J. Sun, L. Du, B. Sun, G. Han, Y. Ma, J. Wang, H. Huo, C. Du and G. Yin, *ACS Appl. Mater. Interfaces*, 2020, **12**, 24717-24725.
32. D. Das, A. Das, M. Reghunath and K. K. Nanda, *Green Chem.*, 2017, **19**, 1327-1335.
33. J. A. Koza, Z. He, A. S. Miller and J. A. Switzer, *Chem. Mater.*, 2012, **24**, 3567-3573.
34. K. Zhu, T. Wu, M. Li, R. Lu, X. Zhu and W. Yang, *J. Mater. Chem. A*, 2017, **5**, 19836-19845.
35. J. Bao, X. Zhang, B. Fan, J. Zhang, M. Zhou, W. Yang, X. Hu, H. Wang, B. Pan and Y. Xie, *Angew. Chem. Int. Ed.*, 2015, **54**, 7399-7404.
36. Y. Wang, Y. Zhang, Z. Liu, C. Xie, S. Feng, D. Liu, M. Shao and S. Wang, *Angew. Chem. Int. Ed.*, 2017, **56**, 5867-5871.
37. X. Miao, L. Wu, Y. Lin, X. Yuan, J. Zhao, W. Yan, S. Zhou and L. Shi, *Chem. Commun.*, 2019, **55**, 1442-1445.
38. J. Wang, J. Liu, B. Zhang, H. Wan, Z. Li, X. Ji, K. Xu, C. Chen, D. Zha, L. Miao and J. Jiang, *Nano Energy*, 2017, **42**, 98-105.
39. T. Ling, D.-Y. Yan, Y. Jiao, H. Wang, Y. Zheng, X. Zheng, J. Mao, X.-W. Du, Z. Hu, M. Jaroniec and S.-Z. Qiao, *Nat. Commun.*, 2016, **7**, 12876.
40. Y. Zhao, C. Chang, F. Teng, Y. Zhao, G. Chen, R. Shi, G. I. N. Waterhouse, W. Huang and T. Zhang, *Adv. Energy Mater.*, 2017, **7**, 1700005.

 This journal is © The Royal Society of Chemistry 20xx

Please do not adjust margins